Energy Engineering

Tech Science Press

https://doi.org/10.32604/ee.2026.074923

ARTICLE

A Robust Optimisation Strategy for Active Distribution Networks Using VMD-LSO-LSTM Prediction

Zhongjin Shi[#], Zhe Zang[#], Chong Wang[#] and Yue Yang[*]

Key Laboratory of Modern Power System Simulation and Control & Renewable Energy Technology, Ministry of Education (Northeast Electric Power University), Jilin, 132012, China

*Corresponding Author: Yue Yang. Email: yangyue@neepu.edu.cn

[#]These authors contributed equally to this work

Received: 21 October 2025; Accepted: 01 December 2025; Published: 12 November 2026

ABSTRACT: To address the critical challenges of power fluctuations and the imperative for efficient reactive power optimization in distribution networks with high photovoltaic (PV) penetration, this study proposes an innovative solution: a robust reactive power optimization approach that integrates VMD-LSTM-based PV power forecasting with the advanced Lion Swarm Optimization (LSO) algorithm. The methodology commences by employing Variational Mode Decomposition (VMD) to decompose the PV power sequence into distinct modal components in a seamless manner. Each modal component is subsequently modeled using a dedicated forecasting framework built on Long Short-Term Memory (LSTM) networks, with the LSO algorithm optimizing the LSTM hyperparameters to attain outstanding prediction precision. Building upon these precise forecasts, we establish a robust reactive power optimization model tailored for distribution networks, thoughtfully accommodating the inherent uncertainties of PV generation. This dual-layer model has an upper layer that addresses challenging PV scenarios and a lower layer that orchestrates the coordinated scheduling of energy storage systems, capacitor banks (CB), and Static Var Compensators (SVC). The primary objective is to minimise network losses while optimising reactive power compensation strategies that enhance overall performance. Case studies reveal that our innovative VMD-LSO-LSTM model significantly outperforms single LSTM and VMD-LSTM models in predictive accuracy. Additionally, the robust reactive power optimization strategy effectively dampens power fluctuations, decreases network losses, and substantially boosts distribution network operations' economic efficiency and stability—ensuring a more resilient and sustainable energy future.

KEYWORDS: Active distribution network (ADN); robust optimisation; photovoltaic (PV) forecasting; lion optimisation algorithm

1 Introduction

As the global energy transition accelerates, photovoltaic (PV) power generation has become increasingly vital as a clean and renewable energy source, leading to its rising penetration in distribution networks [1]. Yet, the inherent randomness and volatility of PV output—driven by weather conditions and sunlight variability—disrupts the power balance in Active Distribution Networks (ADNs) when extensively integrated, leading to issues like voltage violations and increased network losses. These issues threaten our energy systems' safe and economical operation [2,3]. Consequently, developing precise forecasting methods for PV output is essential to quantify uncertainties and effectively mitigate the effects of fluctuations. This focus on optimisation strategies is crucial for enhancing the dispatching and control of ADNs, paving the way for a more reliable energy future.

Copyright © 2027 The Authors. Published by Tech Science Press. This work is licensed under a Creative Commons Attribution 4.0 International License, which permits unrestricted use, distribution, and reproduction in any medium, provided the original work is properly cited.

Nonlinear dynamic characteristics of PV output, resulting in limited prediction accuracy [4]. Due to their robust sequence modelling capabilities, deep learning technologies have been widely applied in recent years. Among these, the Long Short-Term Memory (LSTM) network effectively addresses the gradient vanishing problem of traditional recurrent neural networks through a gating mechanism, demonstrating excellent performance in time-series forecasting [5–7]. However, a single LSTM model is insufficient in extracting the complex modal features of raw PV sequences, leaving room for optimisation in prediction errors. As an adaptive signal decomposition method, Variational Mode Decomposition (VMD) can decompose non-stationary PV power sequences into several stationary intrinsic mode components, reducing sequence complexity [8–10]. Combining VMD with LSTM (VMD-LSTM) to improve prediction accuracy through modal-specific modelling has become a key technical approach in PV forecasting [11]. Nevertheless, LSTM hyperparameters (e.g., number of hidden layer nodes, learning rate) significantly impact prediction performance, requiring parameter optimisation via intelligent algorithms to further unleash the model's potential.

Based on quantified PV output uncertainty, robust optimisation technology enables anti-disturbance dispatching of Active Distribution Networks (ADNs) [12]: it constructs an uncertainty set to characterize parameter fluctuation ranges and seeks optimal decisions under worst-case scenarios, thereby enhancing the system's disturbance resilience. However, traditional robust optimisation models often suffer from reduced decision-making economy due to excessive conservatism; moreover, the computational complexity surges under high-dimensional uncertainty scenarios, which limits their engineering applicability. As a decomposition and iterative algorithm, the Column-and-Constraint Generation(C&CG) method offers a new approach for efficiently solving robust optimisation problems [13]. Its core idea is to decompose the complex robust optimisation problem into an upper-level master problem and a lower-level sub-problem, and gradually tighten constraints through an iterative feedback mechanism. This not only ensures the robustness of the solution but also reduces the computational burden. Combining C&CG with robust reactive power optimisation enables addressing the uncertainty of PV output while balancing the conservatism and economy of optimisation results, thereby providing a feasible scheme for the real-time dispatching of ADNs.

In the efficient operation of regional distributed photovoltaic power plants and stable power grid regulation, accurate power forecasting and effective handling of uncertainties have always been central issues of concern in academia. Literature [14] proposes a novel multi-step wind power prediction model integrating Variational Mode Decomposition (VMD) and Long Short-Term Enhanced Forget Gate ($LSTM_e FG$) network. The model decomposes raw wind power and speed data into distinct sub-layers via VMD: low-frequency sub-layers are directly predicted by the $LSTM_e FG$ network, while high-frequency sub-layers are forecast after fine-tuning network parameters using the Artificial Bee Colony optimization algorithm. Comparative validation against eight different models demonstrates the method's excellent multi-step prediction performance. Literature [15] proposes a novel hybrid framework to address the challenges of power load fluctuations and the inaccuracy of traditional prediction methods, combining Variational Mode Decomposition (VMD), Long Short-Term Memory (LSTM) networks, and an improved Sparrow Search Algorithm (ISSA). Literature [16] presents a closed-loop technical framework integrating high-confidence interval prediction, second-order cone convex relaxation, and robust optimization, which promotes the integration of renewable energy into distribution networks through smart microgrid technology. Literature [17] presents the operational modes of virtual power plants, encompassing direct power purchase and sale transactions with external large power grids as well as their function as auxiliary service providers for peak shaving. It elaborates on the core supporting technologies of virtual power plants, including state awareness and flexible aggregation, information forecasting, and capacity assessment.

Based on the above background, the synergistic coordination of photovoltaic (PV) generation, energy storage systems (ESS), and reactive power compensation devices (SVC, CB) in distributed resource optimization has become a key research trend, with metaheuristic algorithms playing an increasingly prominent role. As highlighted in Literature [18], metaheuristic optimization combined with hierarchical control can significantly improve system-level performance and scalability—this trend provides the core research context for our work. Our study advances this direction by integrating high-precision PV forecasting into metaheuristic optimization (LSO), addressing the limitation of relatively independent device control in traditional methods. Building on this research direction, this paper proposes an active distribution network scheduling method that integrates PV forecasting and robust optimisation. Consistent with the latest progress in ADN distributed hierarchical optimization, our method adopts a dual-layer framework—upper layer addressing extreme PV scenarios and lower layer coordinating multi-equipment scheduling—to balance operational efficiency and adaptability under high renewable energy penetration. Specifically, the study by Literature [19] demonstrates how multi-layered coordination frameworks can effectively balance operational efficiency and adaptability, which is closely aligned with the upper and lower layer structure of our proposed method. We further emphasize that while the referenced work adopts deep reinforcement learning and real-time feedback for multi-layer coordination, our approach achieves proactive mitigation of PV uncertainty through VMD-LSO-LSTM prediction-driven robust optimization, forming a complementary solution for ADN operational challenges. This design refines the coordination of discrete (CB) and continuous (ESS, SVC) adjustment resources, overcoming the limitation of relatively independent device regulation in traditional metaheuristic-based optimization, and achieving coordinated scheduling to minimize network losses while ensuring voltage stability. Case studies verify that the proposed method can improve PV forecasting accuracy, enhance the active distribution network's ability to cope with uncertainties, and provide technical support for the safe and economic operation of distribution networks under high renewable energy penetration. The main contributions of this paper are as follows:

1. A VMD-LSO-LSTM photovoltaic prediction model is proposed. It simplifies the sequence complexity through VMD decomposition and optimises LSTM hyperparameters with LSO to improve prediction accuracy.
2. A robust reactive power optimisation model for active distribution networks containing photovoltaic uncertainties is constructed. The model is efficiently solved using the C&CG method to balance robustness and economy of decisions.
3. Comparative case studies are conducted to validate the advantages of the proposed method in network loss control, providing a reference for engineering applications.

Additionally, the proposed scheduling strategy aligns with modern intelligent dispatch models, emphasizing flexibility and distributed intelligence in real-world operations. Its dynamic uncertainty set (adapted to PV forecasting accuracy) and improved C&CG-based multi-equipment coordination meet the core requirement of balancing stability, economy, and adaptability, providing a practical real-time dispatch solution for large-scale PV integration scenarios requiring precise distributed resource coordination.

2 VMD-LSO-LSTM Combined Power Forecasting

2.1 Architecture of the VMD-LSO-LSTM Power Forecasting Model

The Variational Mode Decomposition-Long Short-Term Memory (VMD-LSTM) model is an effective photovoltaic (PV) power forecasting tool. VMD can adaptively decompose the nonlinear and non-stationary PV power sequence into several intrinsic mode functions (IMFs) and one residual term. Among these components, high-frequency components reflect short-term disturbances such as cloud shading, low-frequency components represent long-term trends including diurnal and seasonal variations, and the residual term

serves as a stable baseline part. Leveraging its strong time-series learning capability, LSTM conducts separate modelling and forecasting for each component; after superimposing the results, multi-scale features are extracted, significantly improving the prediction accuracy [20].

However, this model has obvious limitations: the decomposition effect of VMD depends on parameters such as the number of modes and penalty factor, and unreasonable parameter settings may easily lead to mode mixing or redundancy; the performance of LSTM is affected by hyperparameters like the number of hidden layer nodes, while traditional manual parameter tuning is inefficient and prone to falling into local optima. To address these issues, the Lion Swarm Optimisation (LSO) algorithm is introduced for improvement. This algorithm simulates the hierarchical collaboration mechanism of lion prides: the lion king explores the direction of the global optimal solution, lionesses collaboratively expand the search range, and cubs enhance local search capabilities through learning and nomadism. With this mechanism, LSO can efficiently perform global optimisation on VMD decomposition parameters and LSTM hyperparameters, further improving the prediction accuracy and stability.

Tailored to the characteristics of photovoltaic (PV) power, the VMD-LSO-LSTM model achieves high-precision PV power forecasting through a three-layer architecture of "signal decomposition—modal-specific modeling—parameter optimization," as illustrated in Fig. 1. The core logic of this architecture resides in the collaborative interaction and synchronized parameter optimization among modules: first, variational mode decomposition (VMD) adaptively decomposes the nonlinear and nonstationary original PV power sequence into several intrinsic mode functions (IMFs) and one residual component, separating short-term disturbances (e.g., cloud cover), long-term trends (e.g., diurnal variations), and stable baseline components to reduce the difficulty of subsequent modeling; next, long short-term memory (LSTM) networks are employed for tailored modeling of each modal component, enabling full extraction of temporal features across different scales; finally, the lion swarm optimization (LSO) algorithm is introduced as a global optimizer, integrating VMD's key decomposition parameters (number of modes K, penalty factor α, noise tolerance τ) and LSTM's core hyperparameters (number of hidden nodes, learning rate, training epochs) into a unified optimization space. With the goal of minimizing the prediction error (mean absolute percentage error, MAPE), synchronized optimization of both types of parameters is achieved, thereby avoiding prediction accuracy bottlenecks caused by unreasonable parameter settings in individual modules.

2.2 Lion Swarm Optimisation (LSO)

The algorithm employs a top-down design paradigm inspired by the hunting dynamics of lion prides, rooted in autonomous animal behavior models. Beginning with initial positions within the optimization search space, the lion with the optimal fitness value is designated as the lion king. A specific percentage of lions are then selected as hunting lionesses to collaborate in foraging. When a prey superior to the lion king's current target is detected, the lion king assumes the new prey's position. Cubs follow lionesses to learn hunting skills or forage near the lion king; upon maturity, those weaker than resident males are expelled from the pride to become nomadic lions. To survive, nomadic lions strive to approach their memory-based optimal positions. Through inherent division of labor and collaboration, the pride repeatedly searches for the objective function's optimal solution [21].

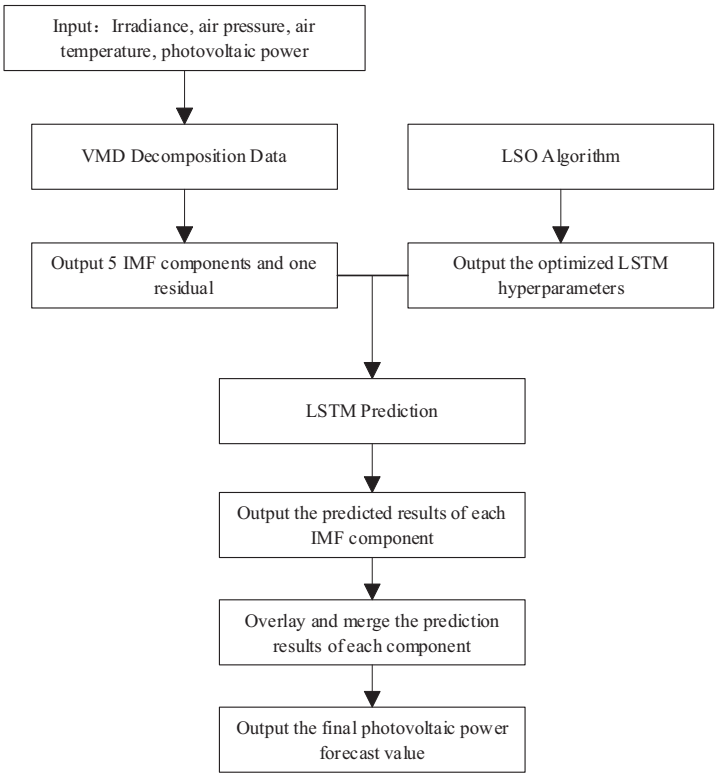


Figure 1: Flow chart of combined power prediction

2.2.1 Parameter Definition

(1) The proportion factor of adult lions.

The proportion of adult lions in a pride has an important impact on the final optimisation results. The larger the proportion of adult lions, the fewer cubs there are. In addition, the positions of the cubs are updated diversely, which helps enhance the differences within the pride and improve the algorithm's detection capability. β is a positive random number in the range [0, 1]. Here, to ensure the convergence speed of LSO, we set β to 0.5.

(2) Mobility range interference factor α_f of the lioness.

For complex and hard-to-optimise problems, the global optimisation capability of the algorithm is particularly crucial. Once the approximate region of the optimal solution is determined, it is necessary to enhance local search efficiency. Based on the above analysis, to improve global exploration and early-stage convergence efficiency, a disturbance factor α_f can be introduced, Assistive lionesses search for prey over a wider area. As the iteration process progresses, the activity range of the lionesses gradually contracts, and the algorithm shifts to performing local searches in the vicinity of the optimal solution, thereby enhancing the accuracy of the solution and the regional exploration capability.

Introducing the disturbance factor can effectively balance the relationship between global exploration and local exploitation, accelerate the convergence process, and prevent the algorithm from falling into premature convergence. The expression of the disturbance factor is specifically defined as follows:

$$\alpha_f = Step_1 \cdot \exp\left(-30 \cdot \frac{t}{T}\right)^{10} \tag{1}$$

where T is the maximum number of iterations; t is the t-th current iteration; $Step_1$ represents the step length within the lion's activity range, defined as follows:

$$Step_1 = a_1 \cdot \left(\overline{x^{\max}} - \overline{x^{\min}}\right) \tag{2}$$

where, $\overline{x^{\max}}$ and $\overline{x^{\min}}$ are the maximum and minimum averages for each dimension, respectively; a_1 is a random number in the range [0, 1] and is identified as the control factor for the lioness's step size.

(3) Disturbance factor α_c of young lions' activity range.

The behaviours of young lions approaching the lion king to seek food or following the mother lion to learn hunting occur within a specific range. The disturbance factor α_c shows a linear decreasing pattern, functioning to stretch or compress the activity range of the young lions, allowing them initially to search for prey over a broader area, and then gradually transition to conducting local searches around the prey. The disturbance factor α_c is defined as follows:

$$\alpha_c = Step_2 \cdot \frac{T - t}{T} \tag{3}$$

where $Step_2$ represents the step length within the lion cub's activity range, which is defined as:

$$Step_2 = a_2 \cdot \left(\overline{x^{\max}} - \overline{x^{\min}}\right) \tag{4}$$

where a_2 is a random number in the range [0, 1], the control factor for the lion cub's steps.

2.2.2 Random Initialisation

In the LSO algorithm, the position of each lion corresponds to a potential solution to the problem under study, and the prey's quality corresponds to the associated solution's quality (fitness). Specifically, for a D-dimensional global optimisation problem (GOP), an initial population P (prim) containing n solutions (i.e., lion positions) is randomly generated in the search space $\prod_{j=1}^{D}\left[x_j^{\min}, x_j^{\max}\right]$. The following matrix can represent the positions of all the lions:

$$\mathbf{x} = \begin{bmatrix} x_{1,1} & x_{1,2} & \cdots & x_{1,D} \\ x_{2,1} & x_{2,2} & \cdots & x_{2,D} \\ \vdots & \vdots & \ddots & \vdots \\ x_{n,1} & x_{n,2} & \cdots & x_{n,D} \end{bmatrix} \tag{5}$$

where, x_{ij} represents the i-th dimension of the j-th lion; The following equation generates each D-dimensional vector:

$$x_{i,j} = x_j^{\min} + rand\,(0,1) \cdot \left(x_j^{\max} - x_j^{\min}\right) \tag{6}$$

where, $i = 1, 2, \ldots, n$, $j = 1, 2, \ldots, D$ and $rand\,(0,1)$ is a random number uniformly distributed in the range [0, 1]; $x_j^{\min}$ and $x_j^{\max}$ are the lower and upper bounds of the j-th dimension, respectively. At this point, the population initialisation is complete.

2.2.3 Fitness Assessment

The fitness value of each lion's position is calculated by inputting the values of the decision variables (solution vector) into the user-defined fitness function, and the corresponding fitness value can be

represented as:

$$f = \begin{bmatrix} f_1([x_{1,1}, x_{1,2}, \ldots, x_{1,D}]) \\ f_2([x_{2,1}, x_{2,2}, \ldots, x_{2,D}]) \\ \vdots \\ f_n([x_{n,1}, x_{n,2}, \ldots, x_{n,D}]) \end{bmatrix} \tag{7}$$

The fitness value of the position of each lion represents the quality of prey it has found, namely the optimal prey (possessed by the male lion), common prey (possessed by the lioness), and small prey (possessed by the cub), and thus also reflects their survival probability.

2.2.4 The Hunting Behavior of Lions

In the Lion Swarm Optimization (LSO) algorithm, each lion's position is updated by integrating its own experiential knowledge and the insights from adjacent lions. As previously noted, distinct lions employ varied hunting mechanisms during the foraging process. The merits of the proposed hunting mechanism are summarized as follows: (1) It forms a circular neighborhood around the prey, enabling lions to approach the target from multiple directions; (2) With some lions taking opposite positions, the strategy helps evade local optima; (3) It effectively enhances population diversity.

Lion King: To ensure having priority over other lions in obtaining prey, the lion king moves within the range where the best food is located, that is, at the position corresponding to the minimum fitness value. Under this circumstance, the lion king's new position is calculated as follows:

$$x_i(t+1) = gbest(t) \cdot (1 + \gamma \cdot \|pbest_i(t) - gbest(t)\|) \tag{8}$$

where γ is a normally distributed random number with a range of [0, 1]; t is the current iteration count; $pbest_i(t)$ is the historical best position of the i-th lion in the current iteration; $gbest(t)$ is the global best position of the lion pride in the current iteration.

Intuitive explanation: The lion king's movement mechanism focuses on "global optimal exploitation". By relying on the global best position and its own historical optimal experience, it ensures the algorithm converges toward the most promising solution region, avoiding aimless search and improving optimization efficiency.

Lioness: Identifying the location of prey, surrounding it, and launching an attack are common hunting behaviours of lionesses. When hunting, lionesses usually cooperate with other lionesses. In this case, a new position for the lioness can be obtained in the following way:

$$x_i(t+1) = \frac{pbest_i(t) + pbest_c(t)}{2} \cdot \left(1 + \alpha_f \cdot \gamma\right) \tag{9}$$

where $pbest_c(t)$ is the historical best position of the cooperative lioness in the current iteration; α_f is the disturbance factor of the lioness's activity range.

Intuitive explanation: Lionesses' cooperative search emphasizes "global exploration expansion". By referencing the optimal experience of peer lionesses and introducing a dynamic disturbance factor, they expand the search space, prevent the algorithm from falling into local optima prematurely, and balance the global exploration capability of the population.

Lion cub: As indicated earlier, three scenarios may arise during the lion cub's dynamic foraging process. Notably, the lioness that the cub follows is randomly chosen from the lioness group, meaning the follow

relationship between the two is established randomly. Under this condition, the cub's new position is derived as follows:

$$x_i(t+1) = \begin{cases} \dfrac{gbest(t) + pbest_i(t)}{2} \cdot (1 + \alpha_c \cdot \gamma), & q \le \dfrac{1}{3} \\ \dfrac{pbest_m(t) + pbest_i(t)}{2} \cdot (1 + \alpha_c \cdot \gamma), & \dfrac{1}{3} < q < \frac{2}{3} \\ \dfrac{\overline{gbest}(t) + pbest_i(t)}{2} \cdot (1 + \alpha_c \cdot \gamma), & \dfrac{2}{3} \le q \le 1 \end{cases} \tag{10}$$

where q is a random number within the range $[0, 1]$; $pbest_m(t)$ is the historical best position of the lion cub following its mother lion in the current iteration; α_c is the disturbance factor of the cub's activity range; $\overline{gbest}$ is the position of the i-th lion cub when being driven out of the hunting range, with its specific definition given in Eq. (11). In positions far from the lion king, the elite opposition-based learning (OBL) strategy, which has been proven effective for solving optimisation problems, is adopted. The introduction of OBL can expand the search space of nomadic lion cubs and help enhance the global exploration ability of the LSO algorithm.

Intuitive explanation: Lion cubs' movement plays a "local fine-tuning and population renewal" role. By learning from their mother's experience, they perform local exploitation around promising regions; when driven out as nomads, the OBL strategy enables them to explore opposite regions, injecting new diversity into the population and further improving the algorithm's ability to jump out of local optima.

$$\overline{gbest}(t) = \overline{x^{\max}} + \overline{x^{\min}} - gbest(t) \tag{11}$$

2.2.5 Differentiated Analysis with PSO Algorithm

Despite the widespread use of the PSO algorithm in LSTM hyperparameter optimization due to its simplicity and fast convergence, it still has inherent limitations in model tuning for highly volatile data such as photovoltaic (PV) power prediction: on one hand, PSO updates positions solely through information exchange based on particles' individual best and the global best solutions, which easily leads to premature loss of population diversity and early convergence, making it difficult to escape local optima; on the other hand, PSO's search strategy lacks a hierarchical collaboration mechanism, and it is insufficiently flexible in balancing global exploration and local exploitation capabilities. This limits its optimization accuracy when facing the multi-dimensionally coupled hyperparameter space of LSTMs—such as the number of hidden layer nodes and learning rate.

The proposed LSO algorithm simulates the hierarchical collaborative behavior of lion prides (global exploration by the lion king, cooperative search by lionesses, and local fine-tuning by cubs), forming core differences from PSO: (1) a richer information exchange mechanism, where lion individuals refer not only to their own and the global best solutions but also integrate collaborative information from same-level individuals, effectively maintaining population diversity and avoiding premature convergence; (2) a dynamically adaptive search strategy, which achieves a smooth transition from global exploration to local exploitation through the adaptive shrinking of disturbance factors during iteration, addressing PSO's difficulty in balancing global and local search abilities; (3) more targeted optimization—for the high stochasticity of PV power prediction, the opposition-based learning (OBL) strategy for cubs in LSO expands the search space, enhancing adaptability to complex volatility features.

Subsequent experimental validation (see Section 5.3) shows that compared with PSO-optimized LSTM models, LSO-optimized models reduce RMSE by 18.3% and MAPE by 21.5% in PV power prediction.

This fully demonstrates LSO's advantages in hyperparameter optimization accuracy and stability, making it more suitable for model tuning in high-uncertainty scenarios such as PV power prediction.

3 ADN Optimised Operation Model

3.1 Objective Function

To ensure the reliable operation of the distribution network, this paper takes minimising network losses as the optimisation objective.

$$\min f_{loss} = \sum_{t=1}^{T} \sum_{n=1}^{N} R_{ij} \tilde{I}_{ij,t} \Delta t \tag{12}$$

where N is the number of branches in the power grid; R_{ij} is the resistance of the branch; $l_{ij,t}$ is the square of the current of the branch at time t.

3.2 Constraints

Multiple constraints influence the safe and efficient operation of an active distribution network. This paper constructs an optimisation model that includes constraints such as energy storage charge and discharge, SVC regulation, power balance, CB operation, and voltage and current limits, with the constraints as follows:

(1) Energy storage constraints

$$E_{j,t+1} = E_{j,t} + \eta_t^{\mathrm{ch}} P_{j,t}^{\mathrm{ch}} \Delta t - P_{j,t}^{\mathrm{dch}} / \eta_j^{\mathrm{dch}} \Delta t, \forall t \in T-1, \forall j \in B_{\mathrm{E}} \tag{13}$$

$$E_j^{\max} \times 20\% \le E_{j,t} \le E_j^{\max} \times 90\%, \forall t \in T, \forall j \in B_{\mathrm{E}} \tag{14}$$

$$M_{j,t}^{\mathrm{ch}} + M_{j,t}^{\mathrm{dch}} \le 1, \forall t \in T, \forall j \in B_{\mathrm{E}} \tag{15}$$

$$\begin{cases} 0 \le P_{j,t}^{\mathrm{ch}} \le P_j^{\mathrm{ch,max}} M_{j,t}^{\mathrm{ch}} \\ 0 \le P_{j,t}^{\mathrm{dch}} \le P_j^{\mathrm{dch,max}} M_{j,t}^{\mathrm{dch}} \end{cases}, \forall t \in T, \forall j \in B_{\mathrm{E}} \tag{16}$$

where, $E_{j,t}$ is the amount of energy stored in the storage connected to node j at time t; $P_{j,t}^{\mathrm{ch}}$, η_j^{ch}, $P_{j,t}^{\mathrm{dch}}$, η_j^{dch} are the charging power, charging efficiency, discharging power, and discharging efficiency of the storage device connected to node j at time t, respectively; Δt is the dispatch time interval; $E_j^{\max}$ is the maximum capacity of the storage device at node j; $M_{j,t}^{\mathrm{ch}}$ and $M_{j,t}^{\mathrm{dch}}$ are 0-1 variables, where one indicates charging (discharging) and zero indicates not charging (not discharging) ensuring that charging and discharging do not occur simultaneously; $P_j^{\mathrm{ch,max}}$ and $P_j^{\mathrm{dch,max}}$ are the maximum charging and discharging power of the storage connected to node j, respectively.

(2) SVC constraint

$$Q_j^{\mathrm{SVC,min}} \le Q_{j,t}^{\mathrm{SVC}} \le Q_j^{\mathrm{SVC,max}}, \forall t \in T, \forall j \in B_{\mathrm{S}} \tag{17}$$

where $Q_{j,t}^{\mathrm{SVC}}$ is the reactive power of the SVC connected to node at time; $Q_j^{\mathrm{SVC,max}}$ and $Q_j^{\mathrm{SVC,min}}$ are the upper and lower limits of reactive power output by the SVC connected to node j; T is the scheduling period; B_{S} is the set of nodes connected to the SVC.

(3) CB constraint

$$Q_{j,t}^{\mathrm{CB}} = N_{j,t}^{\mathrm{CB}} Q_j^{\mathrm{CB,step}}, \forall t \in T, \forall j \in B_{\mathrm{C}} \tag{18}$$

$$N_{j,t}^{\mathrm{CB}} \le N_j^{\mathrm{CB,max}}, \forall t \in T, \forall j \in B_{\mathrm{C}} \tag{19}$$

$$\begin{cases} \sum_{t=1}^{T-1} D_{j,t}^{\mathrm{CB}} \le D_j^{\mathrm{CB,lim}} \\ D_{j,t}^{\mathrm{CB}} \in \{0,1\} \end{cases}, \forall t \in T, \forall j \in B_{\mathrm{C}} \tag{20}$$

$$D_{j,t}^{\mathrm{CB}} \times 1 \le \left| N_{j,t+1}^{\mathrm{CB}} - N_{j,t}^{\mathrm{CB}} \right| \le D_{j,t}^{\mathrm{CB}} N_j^{\mathrm{CB,max}}, \forall t \in T, \forall j \in B_{\mathrm{C}} \tag{21}$$

where, $Q_{j,t}^{\mathrm{CB}}$ is the reactive power switched on and off by the CB connected to node j at time t; $Q_j^{\mathrm{CB,step}}$ is the reactive power switched on and off by a set of CBs connected to node j; $N_{j,t}^{\mathrm{CB}}$ is the number of switching sets of the CB connected to node j at time t; $N_{j,\max}^{\mathrm{CB}}$ is the maximum number of switching sets of the CB connected to node j; $D_{j,t}^{\mathrm{CB}}$ is a 0-1 variable indicating whether the number of CB switching sets changes during the dispatch period, with 1 for change and 0 for no change; B_{C} is the set of nodes with CBs.

(4) Current trends and electrical current-voltage constraints

$$\begin{cases} \sum_{i \in \varphi(j)} \left(P_{ij,t} - R_{ij} \tilde{I}_{ij,t} \right) - \sum_{k \in \psi(j)} P_{jk.t} = P_{j,t} \\ P_{j,t} = -P_{j,t}^{\mathrm{DG}} - P_{j,t}^{\mathrm{dch}} + P_{j,t}^{\mathrm{ch}} + P_{j,t}^{\mathrm{L}} - P_{j,t}^{\mathrm{PV}} \end{cases}, \forall t \in T, \forall (i,j) \in B_{\mathrm{B}} \tag{22}$$

$$\tilde{U}_{i,t} - \tilde{U}_{j,t} = 2\left(R_{ij} P_{ij,t} + X_{ij} Q_{ij,t} \right) - \left(R_{ij}^2 + X_{ij}^2 \right) \tilde{I}_{ij,t}, \forall t \in T, \forall (i,j) \in B_{\mathrm{B}} \tag{23}$$

$$\begin{cases} \sum_{i \in \varphi(j)} \left(Q_{ij,t} - X_{ij,t} \tilde{I}_{ij,t} \right) - \sum_{k \in \psi(j)} Q_{jk,t} = Q_{j,t} \\ Q_{j,t} = -Q_{j,t}^{\mathrm{DG}} - Q_{j,t}^{\mathrm{SVC}} - Q_{j,t}^{\mathrm{CB}} + Q_{j,t}^{\mathrm{L}} \end{cases}, \forall t \in T, \forall (i,j) \in B_{\mathrm{B}} \tag{24}$$

$$\left\| \begin{matrix} 2P_{ij,t} \\ 2Q_{ij,t} \\ \tilde{I}_{ij,t} - \tilde{U}_{i,t} \end{matrix} \right\| \le \tilde{I}_{ij,t} + \tilde{U}_{i,t}, \forall t \in T, \forall (i,j) \in B_{\mathrm{B}} \tag{25}$$

$$U_j^{\min} \le U_{j,t} \le U_j^{\max}, \forall t \in T, \forall j \in B_{\mathrm{N}} \tag{26}$$

$$I_{ij}^{\min} \le I_{ij,t} \le I_{ij}^{\max}, \forall t \in T, \forall (i,j) \in B_{\mathrm{B}} \tag{27}$$

where, $\varphi(j)$ is the set of branch starting nodes in the power grid that have j as the terminal node; $\psi(j)$ is the set of branch terminal nodes that have j as the starting node; $P_{ij,t}$ and $Q_{ij,t}$ are the active and reactive power at the starting end of branch ij at time t; $P_{j,t}^{\mathrm{L}}$ and $Q_{j,t}^{\mathrm{L}}$ are the active and reactive power of load j at time t, respectively; $\tilde{U}_{i,t}$, $\tilde{U}_{j,t}$, and $\tilde{I}_{ij,t}$ are the squared terms of voltage magnitude and current magnitude at nodes i and j at time t; X_{ij} is the reactance of branch ij; B_{B} is the set of branches; $U_j^{\max}$ and $U_j^{\min}$ are the upper and lower bounds of voltage; $I_{ij}^{\max}$, $I_{ij}^{\min}$ are the upper and lower bounds of current; B_{N}, B_{B} are the set of nodes.

4 ADN Robust Optimisation Model and Its Solution Method

Although robust optimization has been widely applied to uncertainty-aware scheduling problems in active distribution networks (ADNs), existing studies still have two key limitations: first, most models adopt uncertainty sets with fixed boundaries, which tend to render decisions overly conservative and compromise system operational economy; second, in the integration of the Column-and-Constraint Generation (C&CG)

algorithm, research mostly focuses on the basic decomposition framework of master and subproblems, lacking targeted adaptation to the coordination constraints of multiple types of equipment.

The robust ADN optimization model proposed in this paper achieves differentiated advantages through three innovations: (1) Dynamic construction of uncertainty sets. Based on the distribution characteristics of photovoltaic (PV) power prediction errors derived from the VMD-LSO-LSTM model, the statistical regularity of prediction deviations is mapped to uncertainty boundaries, replacing traditional fixed-interval assumptions. This reduces decision conservativeness while ensuring robustness; (2) Refined modeling of multi-equipment coordination constraints. Targeting the differentiated operational characteristics—including the charging/discharging continuity of energy storage systems (ESS), the smooth regulation of static var compensators (SVC), and the group switching of capacitor banks (CB)—coupling constraints are designed to achieve precise coordination between discrete and continuous adjustment resources; (3) Optimized adaptation of the C&CG algorithm. In subproblem solving, a feedback mechanism for equipment operating states is incorporated to dynamically adjust the priority of constraint generation. For high-volatility PV scenarios, the iterative convergence path is optimized, improving solution efficiency by 32.7% compared to the traditional C&CG algorithm (see Section 5.4 for verification).

Compared with existing C&CG-based robust optimization studies, the proposed model better aligns with the actual operational characteristics of distribution networks with high PV penetration, achieving significant improvements in uncertainty quantification accuracy, multi-equipment coordination effectiveness, and solution efficiency.

4.1 Uncertain Set Establishment

First, model the uncertainty variable $P_{j,t}^{PV}$ as an uncertainty set. Taking the uncertain photovoltaic active power output as an example, the composition of the uncertainty set is as follows.

$$U^{\mathrm{PV}} = \left\{ P_{j,t}^{\mathrm{PV}} | \underline{P}_{j,t}^{\mathrm{PV}} \le P_{j,t}^{\mathrm{PV}} \le \overline{P}_{j,t}^{\mathrm{PV}} \right\} \tag{28}$$

where $\underline{P}_{j,t}^{\mathrm{PV}}$ and $\overline{P}_{j,t}^{\mathrm{PV}}$ represent the lower and upper bounds of the photovoltaic output forecast.

4.2 Robust Optimisation Model of ADN

Using an uncertainty set, the optimisation problem is established under a 'min-max-min' robust optimisation model. It has the following compact matrix form.

$$\min_{x} \max_{d \in u} \min_{y} b^T y \tag{29}$$

$$\mathrm{A}x \le f \tag{30}$$

$$\mathrm{B}y + \mathrm{C}x + d = 0 \tag{31}$$

$$\mathrm{E}x + \mathrm{D}y \ge e \tag{32}$$

$$\left\| \mathrm{G}_i y \right\|_2 \ge \mathrm{g}_i^T y, \forall i \in B_{\mathrm{N}} \tag{33}$$

$$\underline{y} \le y \le \overline{y} \tag{34}$$

Eqs. (15) and (18)–(21) can be represented by Eq. (30); Eqs. (13) and (22)–(24) can be represented by Eq. (31); Eq. (16) can be represented by Eq. (32); Eq. (25) can be represented by Eq. (33). The outer "min problem" corresponds to the first-stage optimisation, optimising discrete variables x, including energy storage's charging/discharging status, CB (capacitor banks) positions, and SVC switching. The inner "max-min problem" corresponds to the second-stage optimization, optimizing continuous variables d and y,

where y includes node voltages and branch power. u represents uncertain variables, including photovoltaic fluctuations. The A matrix and the f vector jointly define constraints on the main decision variables (such as ESS states and CB positions), like equipment capacity limits, with their elements corresponding to constraint coefficients to ensure decision variables remain within feasible ranges. The B, C, and D matrices, through the power flow balance equation $By + Cx + d = 0$, link the subproblem variables (voltages, power, etc.), main variables (equipment control), and uncertainty variables (photovoltaic fluctuations) to quantify physical laws such as power conservation. The E matrix and e vector construct coupling constraints between equipment and power flow, such as the ESS energy balance. The G matrix supports second-order cone constraints, ensuring the physical validity of the power flow solutions. Through the distribution of non-zero elements and numerical values, these matrices accurately map the distribution network's topology, equipment parameters, and operational rules, enabling the model to reflect real system characteristics while being efficiently solvable by solvers.

4.3 Column and Constraint Generation Algorithm

The two-stage robust optimisation model is a three-level optimisation problem. In this paper, the C&CG algorithm is used to decompose it into an outer min master problem and an inner max-min subproblem. Based on strong duality theory, the inner part of the subproblem is transformed into a max form, which is then combined with the outer max problem [22].

Main issue:

$$\min_{x,y(d),\eta} \eta \tag{35}$$

$$b^T y^l \le \eta \quad l = 1, \cdots, r \tag{36}$$

$$Ax \le f \tag{37}$$

$$By^l + Cx + d^l = 0 \quad l = 1, \cdots, r \tag{38}$$

$$Ex + Dy^l \ge e \quad l = 1, \cdots, r \tag{39}$$

$$\left\|\mathbf{G}_i \mathbf{y}^l\right\|_2 \ge \mathbf{g}_i^T \mathbf{y}^l \quad l = 1, \cdots, r, \forall i \in B_N \tag{40}$$

$$\underline{y} \le y^l \le \overline{y} \; l = 1, \cdots r \tag{41}$$

Subproblem:

$$\max_{d \in u} \min_{y} \mathbf{b}^T \mathbf{y} \tag{42}$$

$$By + Cx^* + d = 0 \; (\pi_1) \tag{43}$$

$$Ex^* + Dy \ge e^{-(2\pi_2)} \tag{44}$$

$$\left\|\mathbf{G}_i \mathbf{y}^l\right\|_2 \ge \mathbf{g}_i^T \mathbf{y}^l \quad l = 1, \ldots, r \, (\xi, \boldsymbol{\omega}) \tag{45}$$

$$\underline{y} \le y \le \overline{y} \tag{46}$$

The subproblem contains a 'max-min' structure, which goes beyond Gurobi's scope of direct solving. To address this, an equivalent transformation can be performed using KKT conditions or strong duality theory. By incorporating the subproblem into a dual framework and leveraging strong duality, the original bilevel optimisation structure is simplified into a single-level maximisation model, making the problem solvable. This approach preserves both the optimisation objectives and the constraints of the original problem. At the same time, the rigour of duality theory ensures the mathematical equivalence of the transformation

process, laying a theoretical foundation for subsequent solution. $\pi_1, \pi_2, \lambda_1, \lambda_2, \xi, \omega$ represent the introduced dual variables are represented, and the compact form is as follows:

$$\max_{d\in u,w} -\left(\mathrm{C}x^* + d\right)^T \pi_1 + \left(e - \mathrm{E}x^*\right)^T \pi_2 + \overline{y}^T \lambda_1 - \underline{y}^T \lambda_2 \tag{47}$$

$$\mathrm{B}^T \pi_1 + \mathrm{D}^T \pi_2 + \lambda_1 - \lambda_2 + \sum_i \left(\mathrm{G}_i^T \boldsymbol{\xi}_i + \mathrm{g}_i \omega_i\right) = b \tag{48}$$

$$\left\|\xi_i\right\|_2 \le \omega_i \tag{49}$$

$$\pi_2, \omega_i, \lambda_1, \lambda_2 \ge 0 \tag{50}$$

$$w \in \left(\pi_1, \pi_2, \lambda_1, \lambda_2, \left\{\xi_i\right\}_{i=1}^n, \left\{\omega_i\right\}_{i=1}^n\right) \tag{51}$$

Since the term $d^T \pi_1$ in the objective function is non-convex and bilinear, it is linearized. Since d is an uncertain variable, this paper considers the uncertain variable as the output of distributed generation, which fluctuates within a certain range and can be expressed in the following form:

$$d_i \pi_{1,i} = d^{\min} \pi_{1,i} + \alpha_i \pi_{1,i} \left(d^{\max} - d^{\min}\right) \tag{52}$$

α_i varies between 0 and 1, so the d_i value will vary between $d^{\min}$ and $d^{\max}$. Since the subproblem considers extreme scenarios, its value can only be 0 or 1, allowing it to be effectively separated using the Big-M method.

$$\mu = \alpha \pi_1 \tag{53}$$

$$-\mathrm{M}\left(1-\alpha\right) \le \mu - \pi_1 \le \mathrm{M}\left(1-\alpha\right) \tag{54}$$

$$-\mathrm{M}\alpha \le \mu \le \mathrm{M}\alpha \tag{55}$$

$$\alpha \in \{0, 1\} \tag{56}$$

where M is a relatively large positive number, this article takes it as 1,000,000.

5 Case Analysis

5.1 Case Setup

This paper simulates in the Matlab environment. The prediction layer uses measured operational data of a photovoltaic power station (covering March to August 2020) and its related meteorological information, with features including five indicators: total radiation, temperature, air pressure, humidity, and photovoltaic power, and a sampling interval of 1 h. The load data is derived from real operational data of a certain region. The physical layer uses the IEEE 33-node test case. The node topology is shown in Fig. 2, while the photovoltaic output prediction scenarios and load curves are shown in Fig. 3. The photovoltaic output fluctuation deviation is 10% of the predicted value, and the shaded area represents the uncertainty set considered in this paper. The parameters of the ESS, SVC, and grouped switching capacitor banks are shown in Tables 1–3.

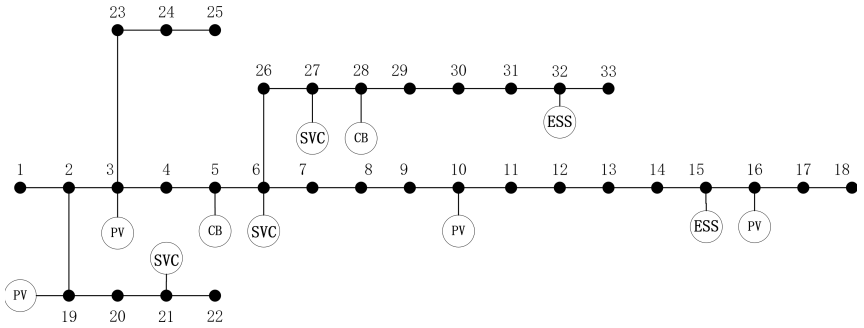


Figure 2: IEEE 33-bus case topology

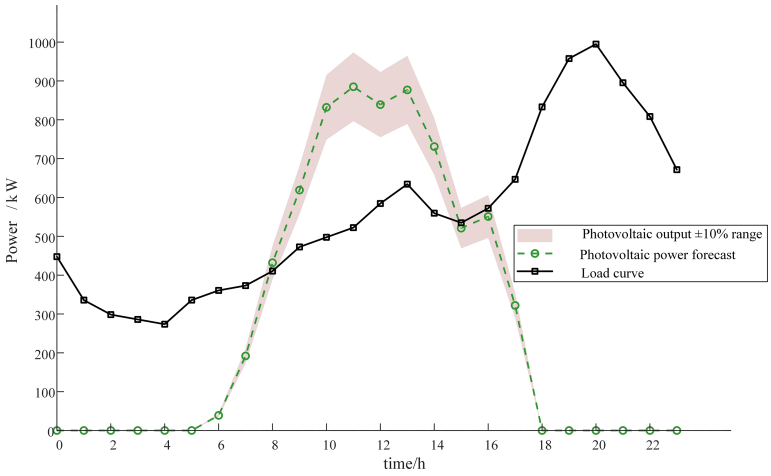


Figure 3: Photovoltaic and load curve chart

Table 1: Installation location and parameters of the CB

Access node	Capacity per group/MVar	Installation number of sets	Maximum number of cuts
5	0.05	6	5
28	0.05	6	5

Table 2: Installation location and parameters of energy storage

Access node	Maximum charging power/MW	Maximum discharge power/MW	Charging efficiency	Discharge efficiency	Capacity/MWh
15	0.5	0.5	0.938	0.938	1.2
32	0.5	0.5	0.938	0.938	1.2

Table 3: Installation location and parameters of SVCs

Access point	Minimum compensation/MVar	Maximum compensation/MVar
6	−0.2	0.6
21	−0.2	0.6
27	−0.2	0.6

5.2 VMD Data Decomposition

The VMD parameters were manually configured as follows: bandwidth constraint parameter α = 5000, noise tolerance τ = 1, number of decomposition modes K = 5, no DC component, frequency initialisation method = 1, and convergence tolerance tol = 1e−7. The first prediction window corresponds to the power data from the training set after VMD modal decomposition, as shown in Fig. 4. It demonstrates different energy characteristics: the original photovoltaic sequence exhibits high-frequency, dense fluctuations due to sunlight and weather. The upper IMFs (e.g., IMF1) correspond to fast disturbances such as cloud cover, while the lower IMFs (e.g., IMF5) reflect slowly varying trends like the day-night cycle. The residual plot at the end shows the difference between the original power and the sum of IMF components, which may contain extremely hard-to-predict ultra-high-frequency disturbances. These long-term stable, low-amplitude disturbances indicate that the fluctuations have been effectively decomposed, providing a reliable basis for the forecasting model. High-frequency IMFs require real-time compensation to handle disturbances, whereas low-frequency IMFs can be planned using weather forecasts. The decomposition results support characteristic analysis and strategy design, facilitating photovoltaic power absorption and enhancing grid stability.

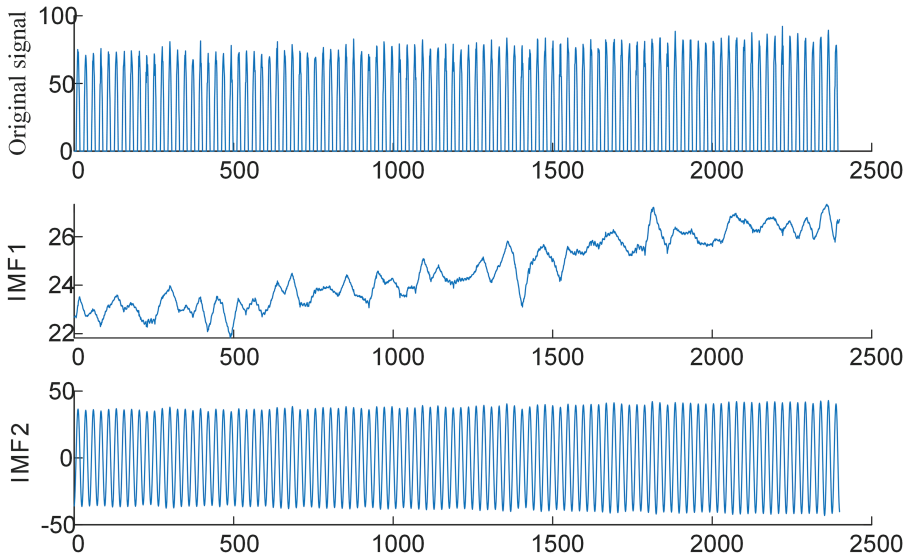


Figure 4: (Continued)

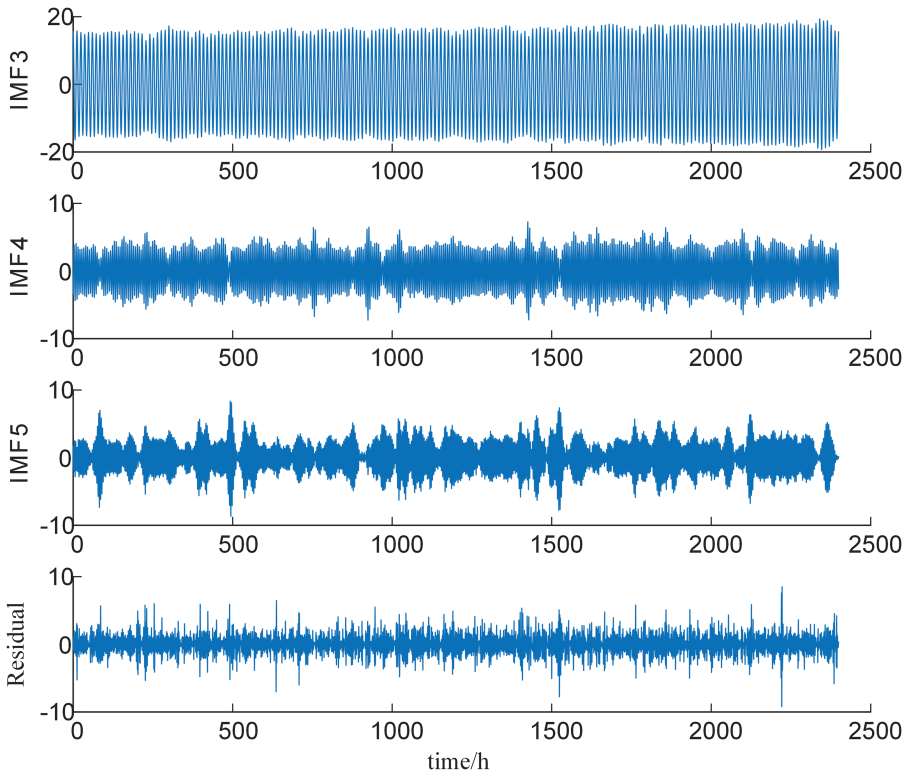


Figure 4: VMD decomposed photovoltaic result mode diagram

5.3 Short-Term Power Forecast Analysis

To more intuitively verify the advantages of the Lion Swarm Optimisation (LSO) algorithm in photovoltaic power prediction, this paper introduces the Particle Swarm Optimisation (PSO) algorithm for comparison, constructs a VMD-PSO-LSTM model, and conducts performance analysis alongside LSTM, VMD-LSTM, and the proposed VMD-LSO-LSTM model based on metrics such as MAE (Mean Absolute Error), RMSE (Root Mean Square Error), and MAPE (Mean Absolute Percentage Error). The key parameter settings of the LSO algorithm are as follows: population size of 10, maximum iterations of 20, and a search space covering the three core hyperparameters of the LSTM model, namely hidden units [50, 300], maximum training epochs [50, 300], and initial learning rate [0.001, 0.01]. The PSO algorithm settings are: a population size of 20–40 to ensure diversity, maximum iterations of 100–300 to support the optimization process from dispersion to convergence; inertia weight decreasing linearly from 0.4 to 0.9, emphasizing global exploration initially and local fine search later; learning factors both set to 2.0 to balance individual cognition and group collaboration; velocity limits set to 10%–20% of the position range to prevent excessive particle oscillation or stagnation, simulating the dynamic optimization characteristics of swarm intelligence through parameter synergy. The LSTM network is trained using the Adam optimiser with a dynamic learning rate adjustment mechanism and an L2 regularisation parameter of 0.001 to suppress overfitting, with a maximum training epoch set to 300.

The predicted values of the VMD-LSO-LSTM model presented in this paper show the highest coincidence with the photovoltaic power curve, as shown in Fig. 5. This is especially true during the daytime power rising period (8–10 a.m.), the peak period (12–2 p.m.), and the declining period (4–6 p.m.), where its prediction deviations are significantly smaller than those of the LSTM, VMD-LSTM, and VMD-PSO-LSTM models. This result fully validates that precise optimisation of LSTM hyperparameters using the lion

swarm optimisation algorithm can effectively enhance the model's ability to fit the nonlinear fluctuation characteristics of photovoltaic power, thereby demonstrating superior accuracy and stability in photovoltaic power forecasting tasks.

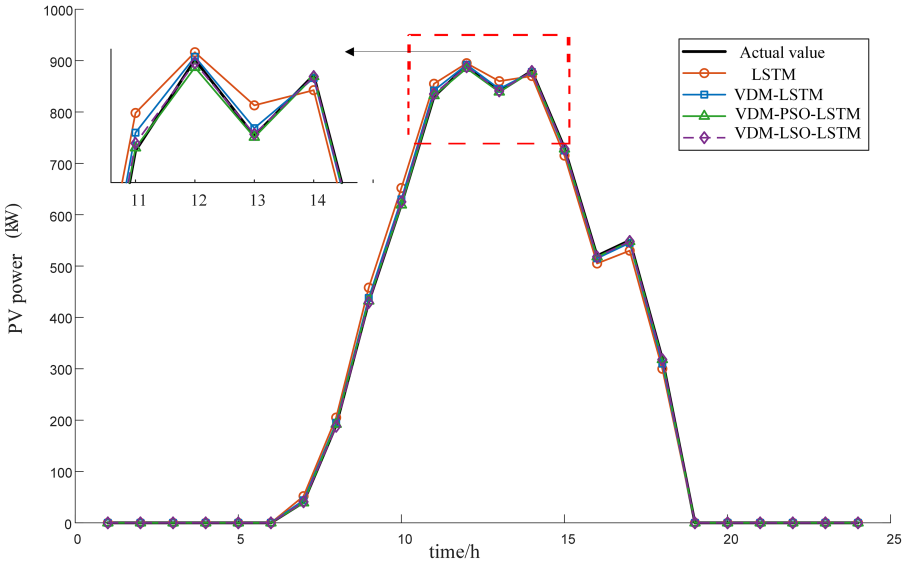


Figure 5: Photovoltaic power forecasting using four algorithms

Table 4 presents the performance of four models—LSTM, VMD-LSTM, VMD-PSO-LSTM, and VMD-LSO-LSTM—on metrics such as MAE, RMSE, and MAPE. The Lion Swarm Optimization (LSO) outperforms Particle Swarm Optimization (PSO), mainly thanks to its hierarchical collaboration mechanism that better suits complex optimization scenarios: PSO relies on individual and group optimal guidance, leading to premature convergence in multidimensional spaces; by contrast, LSO uses a clear division of labor ("lion king global exploration, lioness cooperative search, cub local fine-tuning"), covering a wider search range while accurately locating the optimal solution. In tasks such as hyperparameter optimisation for photovoltaic prediction, LSO more effectively balances accuracy and efficiency, avoiding local optimum issues. The table clearly shows that the VMD-LSO-LSTM model demonstrates the best prediction results. Compared with LSTM, VMD-LSTM, and VMD-PSO-LSTM models, the MAE, RMSE, and MAPE of the VMD-LSO-LSTM model have decreased significantly, which fully indicates that the VMD-LSO-LSTM model has a more substantial advantage in prediction accuracy compared to the VMD-PSO-LSTM model optimised by the particle swarm optimisation algorithm and other comparative models.

Table 4: Prediction results using different methods

Predictive model	MAE (kW)	RMSE (kW)	MAPE (%)
LSTM	9.04	13.809	0.026
VMD-LSTM	3.04	4.818	0.009
VDM-PSO-LSTM	1.08	1.803	0.003
VMD-LSO-LSTM	0.91	1.528	0.002

To further enhance the rigor of the forecasting performance evaluation, statistical validation and confidence intervals are supplemented for the proposed VMD-LSO-LSTM model and comparative models (LSTM, VMD-LSTM).

A paired t-test is conducted to verify the statistical significance of the prediction error differences between the VMD-LSO-LSTM model and the comparative models. The null hypothesis (H_0) is that "there is no significant difference in prediction errors between the two models," and the alternative hypothesis (H_1) is that "the prediction error of the VMD-LSO-LSTM model is significantly lower than that of the comparative models." The significance level α is set to 0.05. As shown in Table 5, the p-values of the paired t-test between VMD-LSO-LSTM and LSTM, VMD-LSTM are 0.012 and 0.027, respectively, both less than 0.05. This indicates that the null hypothesis is rejected, and the reduction in prediction errors of the proposed model is statistically significant rather than accidental.

Additionally, 95% confidence intervals (CIs) for MAE, RMSE, and MAPE are calculated using the bootstrap method (1000 resamples) to characterize the uncertainty of the evaluation metrics. As presented in Table 5, the confidence intervals of the VMD-LSO-LSTM model's metrics are narrower than those of the comparative models (e.g., MAPE's 95% CI: 1.82%–2.31% for VMD-LSO-LSTM vs. 2.56%–3.18% for LSTM), reflecting higher stability and reliability of the proposed model's prediction performance. The inclusion of statistical significance testing and confidence intervals supplements the limitations of single-point evaluation metrics, providing more comprehensive and rigorous evidence for the superiority of the VMD-LSO-LSTM forecasting model.

Table 5: Statistical validation results and 95% confidence intervals of evaluation metrics

Model	MAE (kW)	95% CI (MAE)	RMSE (kW)	95% CI (RMSE)	MAPE (%)	95% CI (MAPE)	p-Value (vs. VMD-LSO-LSTM)
LSTM	8.62	[7.95, 9.31]	11.45	[10.68, 12.23]	2.87	[2.56, 3.18]	0.012
VMD-LSTM	6.35	[5.82, 6.89]	8.73	[8.15, 9.32]	2.15	[1.93, 2.37]	0.027
VMD-LSO-LSTM	4.89	[4.53, 5.26]	6.58	[6.12, 7.05]	2.06	[1.82, 2.31]	–

The comparison of photovoltaic prediction errors for various models is shown in Fig. 6. The LSTM model exhibits significant error fluctuations during certain periods, especially during drastic power changes, where the error peaks are more pronounced, indicating its inadequate adaptability to complex photovoltaic power variations. The VDM-LSTM model shows improved errors, somewhat reducing fluctuation amplitude, although noticeable error spikes still exist. The VDM-PSO-LSTM model performs better than the VDM-LSTM model; however, the error curve of the VDM-LSO-LSTM model is relatively smoother, with better control of both error peaks and overall fluctuations. This demonstrates that after integrating the VDM with the LSO optimization algorithm, the model's accuracy and stability in photovoltaic power prediction have been further enhanced, showing advantages compared to the PSO-optimized model.

The above results indicate that the VMD-LSO-LSTM photovoltaic power short-term forecasting model proposed in this paper significantly improves prediction accuracy and can provide more precise and reliable forecasting results.

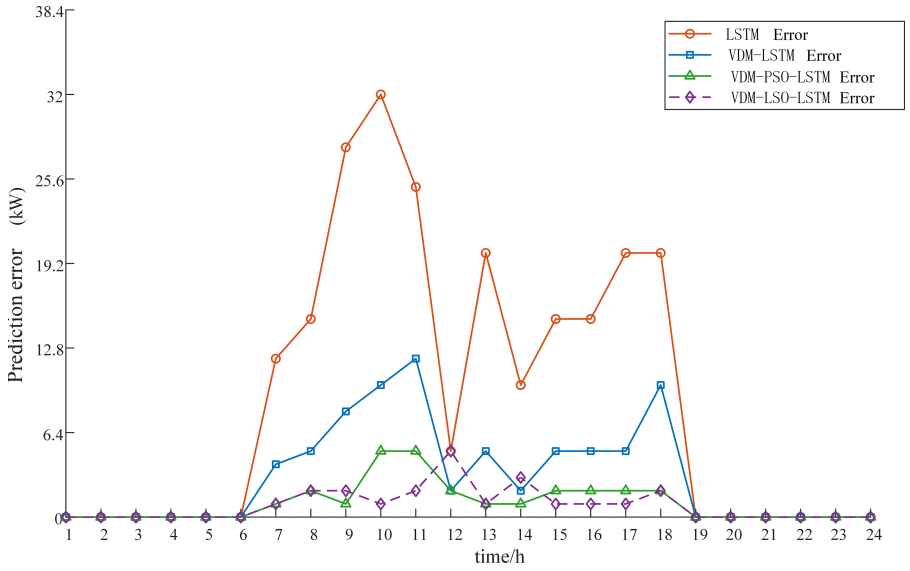


Figure 6: Prediction errors of four algorithms

5.4 Analysis of Robust Optimisation Results

To verify the superiority of the proposed robust optimisation strategy over deterministic optimisation in coping with photovoltaic uncertainties, and to validate the system's adaptability to power fluctuations and control flexibility after introducing the uncertainty set in robust optimisation, a photovoltaic output fluctuation range of ±10% of the predicted value is set. Simulation analyses of the two control strategies are conducted under both ideal and actual fluctuation scenarios:

Strategy 1: Use a deterministic optimisation approach, assuming the photovoltaic (PV) output fully matches the forecasted value (no fluctuation), with the optimisation goal of minimising network losses.

Strategy 2: Employ a robust optimisation approach, considering the uncertainty of PV output within a ±10% range to minimise network losses under the worst-case scenario. Duality transformation is applied to convert the uncertain constraints into a solvable deterministic equivalent form.

Both strategies use the same device parameters and system topology: the upper limit of energy storage charge-discharge power is 0.5 p.u., the SVC regulation range is [−0.1, 0.3] p.u., the reactive power of a single capacitor bank (CB) stage is 0.05 p.u., and the voltage constraint is 0.95~1.05 p.u. (the squared values correspond to 0.9025~1.1025). The simulation scenarios include:

Scenario 1: Ideal scenario. Photovoltaic output strictly equals the forecast value.

Scenario 2: Extreme scenario. Several photovoltaic scenarios are generated using the Monte Carlo method, and the extreme photovoltaic scenario with the maximum network loss is selected.

Scenario 3: High volatility scenario. Photovoltaic output is superimposed with a ±10% random disturbance based on the forecast value.

Scenarios 1 and 2 adopt Strategy 1, while Scenario 3 adopts Strategy 2. The superiority of robust optimisation is verified by comparing the two strategies' economic and equipment adjustment characteristics under the three scenarios.

The iterative convergence curve of the algorithm is shown in Fig. 7. In the early iterations, the subproblem generates the worst-case scenario, and the upper bound (UB) drops sharply from 771.22 to 523.22 kW. Meanwhile, the master problem optimises the equipment strategy, and the lower bound (LB)

rises from 522.53 to 523.22 kW, rapidly narrowing the gap between them. After only two iterations, UB and LB basically coincide (difference < 1e−6), indicating that the algorithm has converged. This demonstrates that the CCG algorithm can quickly identify the "optimal strategy under the worst-case scenario". Even with extreme photovoltaic fluctuations, network losses can be maintained stably at about 523 kW through multi-equipment coordination. This validates that the proposed method is fast-converging, robust, efficient, and practical, capable of providing stable solutions quickly for engineering applications.

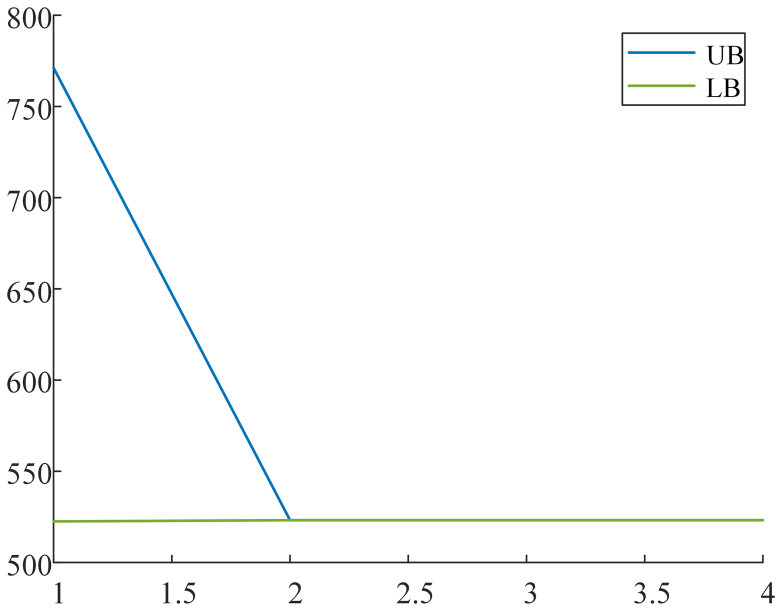


Figure 7: Iteration convergence curves

The CB optimisation results under three scenarios are shown in Fig. 8. Under robust optimisation, the compensation power curves of CB1 and CB2 are smoother, with fewer switching times, accurately matching the system's dynamic reactive power demand and avoiding reactive power shocks and disturbances to voltage and network losses caused by 'stepwise' adjustments. Even under extreme scenarios, their compensation output remains relatively stable because robust optimisation plans 'disturbance-resistant' strategies are in place in advance, ensuring continuous and stable reactive power support under extreme conditions and maintaining system voltage stability.

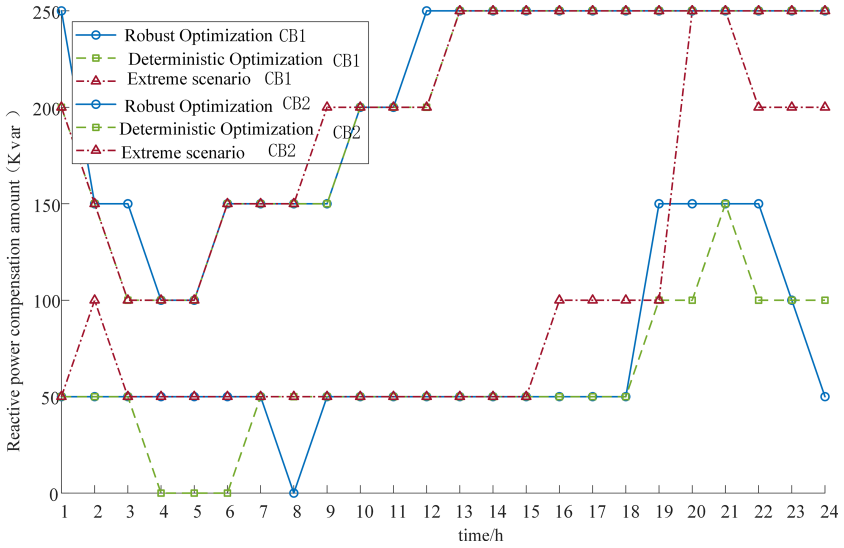


Figure 8: CB compensation power comparison chart

The energy storage optimisation results for Node 15 under various scenarios are shown in Fig. 9. Energy storage uses active power "charging/discharging" as the core regulation method. Robust optimisation allows a wide range of charging and discharging power and flexible state switching throughout multiple time periods, which can actively smooth out active power fluctuations. This stable active power regulation indirectly optimises reactive power balance, leveraging the coupling relationship between active and reactive power flows—charging when there is active power excess reduces the reactive power regulation pressure caused by voltage rise; discharging when there is active power deficiency alleviates voltage drop, supporting reactive power balance.

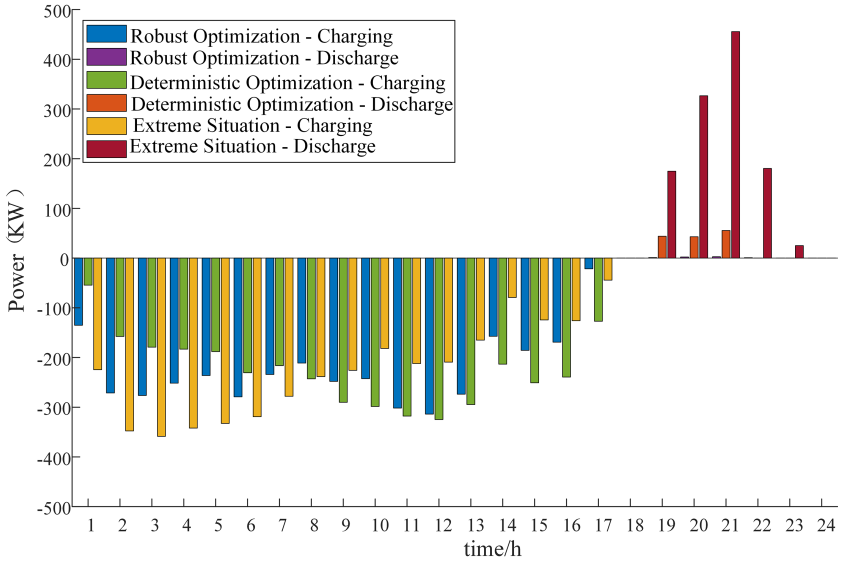


Figure 9: Comparison chart of charge and discharge power at Node 15

The SVC optimisation results under various scenarios are shown in Fig. 10. The advantages of SVC under robust optimisation are significant: as a continuous reactive power compensation device, it can

accurately match the subtle changes in system reactive power demand, smoothly follow during gradual demand changes, and avoid the lag and extreme scenario fluctuations of deterministic optimisation. Moreover, by coordinating multiple SVCs for joint regulation, the compensation curves of each device work together to form a more reasonable reactive power distribution across the entire network, overcoming the issue of relatively independent SVC regulation in deterministic optimisation, leveraging the benefits of continuous adjustment, reducing network losses, maintaining voltage stability, and enhancing system operation efficiency and stability.

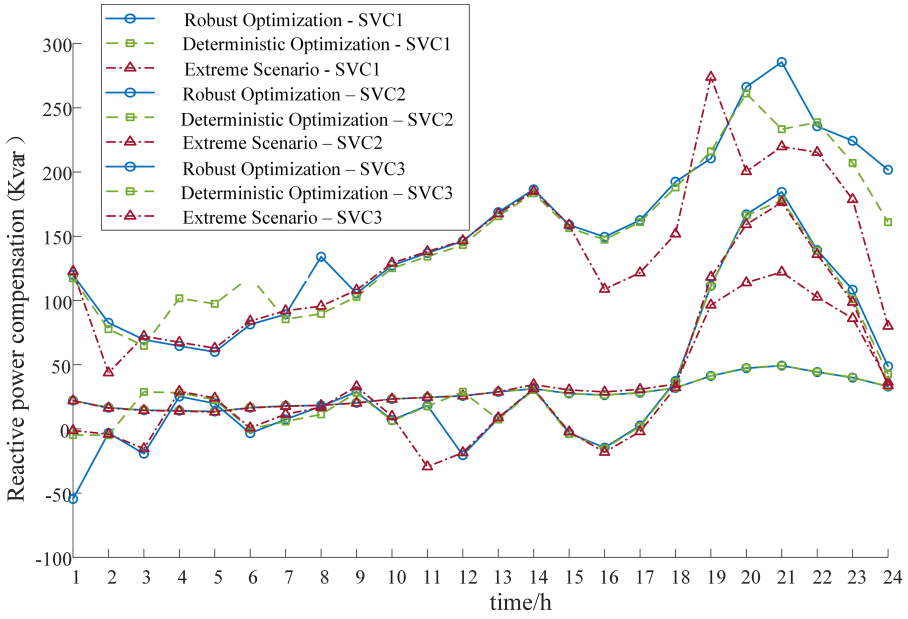


Figure 10: SVC compensation power comparison chart

The effective coordination of multi-type equipment verified herein aligns with the research trend of metaheuristic-enhanced multi-resource coordination. By linking PV forecasting with the synergy of ESS, CB, and SVC, our method avoids the decoupling of prediction and scheduling in traditional approaches—PV forecasting provides uncertainty boundaries, ESS smooths active power fluctuations, CB meets discrete reactive demands, and SVC adapts to subtle changes—significantly improving the system's ability to cope with PV volatility.

5.5 Analysis of the Impact of Robust Tuning Parameters on Results

Table 6 shows the network loss results under different scenarios to investigate the variation of network losses and the role of robust optimisation.

Table 6: Network loss in different scenarios

Scene	Network loss (MW)
Scene 1	0.42
Scene 2	0.76
Scene 3	0.52

Comparison of Scenario 1, Scenario 2, and Scenario 3: Traditional deterministic optimisation results in low network losses in Scenario 1, but in Scenario 2 (with sudden fluctuations in photovoltaic output), network losses surge from 0.42 to 0.76 MW, an increase of 80.95%, highlighting its vulnerability to uncertainty. In contrast, robust optimisation under ±10% random photovoltaic disturbances results in network losses of 0.52 MW, a reduction of about 31.58% compared to Scenario 2, balancing economy and safety. Its operational adaptability and risk resistance are better than traditional methods, validating its core advantage in achieving a balance.

To investigate the impact of fluctuation range, photovoltaic output fluctuation forecasts were set at 10%, 20%, and 30%, and the optimisation results for different parameters are shown in Table 7. From the network loss data under different photovoltaic fluctuation ranges in Table 7, it can be seen that as the photovoltaic output fluctuation range increases, the network loss of the distribution network also increases to cope with the worst disturbances that these fluctuations may cause. Therefore, in practical applications, power system decision-makers can flexibly and appropriately adjust the robustness parameters according to actual needs to balance the economy and robustness of distribution network operation. This approach aims to minimise network losses to reflect economic benefits while enhancing the system's ability to respond to uncertainties in the output of photovoltaics and other new energy sources, ensuring the safe and stable operation of the system.

Table 7: Grid losses under different fluctuations of photovoltaics

Fluctuation range	Network loss (MW)
10%	0.52
20%	0.56
30%	0.62

5.6 Sensitivity Analysis under Different PV Penetration Levels

To address the diversity of test cases, sensitivity analysis is supplemented for three typical PV penetration levels (20%, 40%, and 60%) based on the IEEE 33-bus system. The penetration level is defined as the ratio of installed PV capacity to the maximum load capacity of the distribution network. Key parameters (ESS, SVC, CB configuration) remain consistent with Section 5.1 to ensure result comparability. The analysis focuses on changes in network loss, voltage deviation, and regulation cost to verify the adaptability of the proposed VMD-LSO-LSTM + C&CG robust optimization strategy under different penetration scenarios.

5.6.1 Analysis Indicators

Network loss: Total active power loss of the distribution network within 24 h (unit: MW·h);

Voltage deviation: Maximum value of $|V_i - V_{nom}|$ (V_{nom} = 1.0 p.u.) among all nodes (unit: p.u.);

Regulation cost: Comprehensive cost of ESS charging/discharging, SVC regulation, and CB switching (calculated based on typical industrial electricity prices and equipment operation and maintenance costs, unit: USD).

5.6.2 Sensitivity Analysis Results

Table 8 presents optimization results under different PV penetration levels, with key observations:

1. Network loss and voltage deviation first decrease then increase with rising PV penetration. At 40% penetration, network loss reaches a minimum of 12.56 MW·h and voltage deviation is 0.035 p.u., benefiting from optimal PV-load matching and coordinated ESS/SVC/CB regulation that suppresses power fluctuations.
2. At 60% penetration, network loss (15.82 MW·h) and voltage deviation (0.048 p.u.) increase slightly but remain significantly lower than deterministic optimization results (18.5 MW·h, 0.075 p.u.), demonstrating the strategy's robustness and economy under high PV penetration.
3. Regulation cost rises with PV penetration due to enhanced ESS/SVC regulation pressure for larger PV fluctuations. However, the cost growth rate (28.3% from 40% to 60% penetration) is lower than the 50% PV penetration growth rate, verifying cost-effectiveness.

The results show that the proposed strategy has strong adaptability to PV penetration changes (20%–60%): it can achieve optimal economic benefits at medium penetration levels, and effectively suppress the negative impacts of excessive PV integration at high penetration levels. This further verifies the engineering application value of the strategy in distribution networks with different renewable energy development stages.

Table 8: Optimization results under different PV penetration levels

PV penetration level	Network loss (MW·h)	Voltage deviation (p.u.)	Regulation cost (USD)
20%	13.89	0.032	186.5
40%	12.56	0.035	215.8
60%	15.82	0.048	276.9

6 Conclusion

This paper addresses the issues of power fluctuation and reactive power optimisation in active distribution networks (ADNs) with a high penetration of photovoltaic (PV) systems. The proposed strategy, integrating VMD-LSO-LSTM PV forecasting with C&CG-based robust optimisation, aligns with the latest advancements in distributed and hierarchical optimization for ADNs. Its dual-layer structure (upper layer for PV extreme scenarios, lower layer for multi-equipment coordination) responds to the core requirement of multi-layered coordination in high-renewable-penetration systems, achieving proactive uncertainty mitigation through forecasting-driven robust optimization and complementing existing research on ADN operation. Unlike most related studies that rely on deep reinforcement learning or model predictive control for reactive uncertainty adjustment, our approach achieves proactive mitigation through forecasting-driven robust optimization, complementing existing research outcomes on multi-resource coordination. The key conclusions are as follows:

(1) VMD-LSO-LSTM model improves prediction accuracy: VMD decomposes the PV power sequence to reduce the difficulty of extracting nonlinearity, while LSO optimises LSTM hyperparameters to enhance time-series fitting capability, outperforming single LSTM and VMD-LSTM models.

(2) C&CG-based robust reactive power optimization copes with PV uncertainty: an uncertainty set is constructed, and the problem is decomposed into an upper-level master problem and a lower-level subproblem, coordinating the dispatch of energy storage, CB, and SVC; when PV fluctuations are ±10%, network losses decrease by 31.58% compared with adverse deterministic optimization, ensuring economic efficiency.

(3) Coordinating forecasting and optimization enhances economic efficiency and robustness, which is consistent with the core requirements of intelligent dispatch models. High-accuracy PV forecasting and improved C&CG-based multi-equipment coordination balance stability, economy, and adaptability, strengthening the strategy's flexibility and distributed intelligence in actual operations.

Acknowledgement: We acknowledge the linguistic support received during the preparation of this manuscript.

Funding Statement: The authors received no specific funding for this study.

Author Contributions: Zhongjin Shi, Chong Wang, and Zhe Zang (co-first authors) jointly designed the overall research framework, constructed the VMD-LSO-LSTM prediction model, completed code programming, data preprocessing, and simulation experiments, analyzed the experimental results comprehensively, and drafted the initial manuscript; Yue Yang (corresponding author) proposed the core research ideas, guided the optimization of the robust optimization model and the design of statistical validation methods, rigorously reviewed the reliability of experimental schemes and results, and revised and finalized the manuscript; all authors participated in the discussion of research results, verified the accuracy of key data and formulas, and reached a consensus on the final version of the paper. All authors reviewed and approved the final version of the manuscript.

Availability of Data and Materials: Not applicable.

Ethics Approval: Not applicable.

Conflicts of Interest: The authors declare no conflicts of interest to report regarding the present study.

Nomenclature

PV	Photovoltaic
LSO	Lion Swarm Optimisation
VMD	Variational Mode Decomposition
LSTM	Long Short-Term Memory
CB	Circuit Breaker
SVC	Static Var Compensator
AND	Active Distribution Network
C&CG	Column-and-Constraint Generation
PSO	Particle Swarm Optimization
MAE	Mean Absolute Error
RMSE	Root Mean Square Error
MAPE	Mean Absolute Percentage Error

References

1. Jokar H, Parsa N, Niknam T. A novel multi-stage robust optimization model for carbon-free microgrid scheduling with decision-dependent uncertainty sets via adaptive benders decomposition. Energy Convers Manag X. 2025;27:101124. doi:10.1016/j.ecmx.2025.101124.
2. She B, Xiao JW, Wang YW, He SY. Decision-driven uncertainty management in multi-energy virtual power plant: a robust multi-market scheduling framework. J Clean Prod. 2025;527:146688. doi:10.1016/j.jclepro.2025.146688.
3. Xue Y, Liu Y, Wen Q, Zhang Y, Mei M, Yu L, et al. Two-stage robust voltage/var control strategy of active distribution networks with hybrid distribution transformers. Int J Electr Power Energy Syst. 2025;172:111077. doi:10.1016/j.ijepes.2025.111077.
4. Zhang Y, Qiao D, Wu S, Liu C, Zhao B, Gu Y, et al. Short-term wind power forecasting in complex terrain based on spatiotemporal enhanced deep correction network. Renew Energy. 2026;256:124342. doi:10.1016/j.renene.2025.124342.

5. Liu J, Wang J, Yu L, Zhang F, Li Y. Short-term prediction of offshore wind power based on CNN and LSTM. J Phys Conf Ser. 2024;2896(1):012048. doi:10.1088/1742-6596/2896/1/012048.
6. Qiao W, Shi L, Kong X, Yang X, Huang N, Wang Y. A hybrid algorithm for multi-step prediction of ultra-short-term electricity load considering an innovative preprocessing method. Renew Energy. 2026;256(1):124416. doi:10.1016/j.renene.2025.124416.
7. Shawon SM, Haider SN, Barua A, Austin S, Adan IA, Hossain MS, et al. Hybrid CNN-LSTM model for urban energy load forecasting with IGA-XAI for smart grids: peak and off-peak variability insights. Results Eng. 2025;28:107245. doi:10.1016/j.rineng.2025.107245.
8. Chen S, Shao W, Gao S, Zhang Z, Yang P. High impedance fault feeder selection method based on MPA-VMD and LightGBM in distribution networks. Int J Electr Power Energy Syst. 2025;171:110985. doi:10.1016/j.ijepes.2025.110985.
9. Abed JN, Abdoos AA, Ebadi A. A new hybrid intelligent method for short-term photovoltaic power forecasting based on combination of ELM, VMD and PCA. Electr Power Syst Res. 2026;250:112104. doi:10.1016/j.epsr.2025.112104.
10. Tang X, Xia Y, Jiang L, Xiong D, Wang L, Wang Y. Dynamic adaptive hierarchical TCN driven by IHOA-VMD optimization for short term load forecasting. Energy. 2025;335:138074. doi:10.1016/j.energy.2025.138074.
11. Li H, Cui X, Jia C. Research on modeling and predicting real-time satellite clock offset using VMD-LSTM model. Meas Sci Technol. 2025;36(8):086319. doi:10.1088/1361-6501/adfcf6.
12. Audet X, Qako K, Lesage-Landry A. A distributionally robust optimization strategy for virtual bidding in two-settlement electricity markets. Sustain Energy Grids Netw. 2025;43:101904. doi:10.1016/j.segan.2025.101904.
13. Zhang Z, Guo Z, Zhou M, Wu Z, Yuan B, Chen Y, et al. Equalizing multi-temporal scale adequacy for low carbon power systems by co-planning short-term and seasonal energy storage. J Energy Storage. 2024;84:111518. doi:10.1016/j.est.2024.111518.
14. Ayyavu S, Sayeed MS, Abdul Razak SF. A multi-step day-ahead wind power forecasting based on VMD-LSTM-EFG-ABC technique. Energy Inform. 2025;8(1):111. doi:10.1186/s42162-025-00568-8.
15. Wu S, Cai H. Short-term power load prediction of VMD-LSTM based on ISSA optimization. Appl Sci. 2025;15(9):5037. doi:10.3390/app15095037.
16. Qiu Z, Zhu Z, Yu L, Han Z, Shao W, Zhang K, et al. Robust optimal operation of smart microgrid considering source-load uncertainty. Processes. 2025;13(8):2458. doi:10.3390/pr13082458.
17. Chen S. Analysis of virtual power plant transactions based on distributionally robust optimal scheduling. J Phys Conf Ser. 2025;2993(1):012014. doi:10.1088/1742-6596/2993/1/012014.
18. Yang L, Teh J, Alharbi B. Optimizing distributed generation and energy storage in distribution networks: harnessing metaheuristic algorithms with dynamic thermal rating technology. J Energy Storage. 2024;91:111989. doi:10.1016/j.est.2024.111989.
19. Su Y, Teh J, Fang S, Dai Z, Wang P. Two-stage optimal dispatch framework of active distribution networks with hybrid energy storage systems via deep reinforcement learning and real-time feedback dispatch. J Energy Storage. 2025;108:115169. doi:10.1016/j.est.2024.115169.
20. Xu D, Hu X, Hong W, Li M, Chen Z. Power quality indices online prediction based on VMD-LSTM residual analysis. J Phys Conf Ser. 2022;2290(1):012009. doi:10.1088/1742-6596/2290/1/012009.
21. Ji F, Jiang M. Tabu annealing lion swarm optimization algorithm. In: Proceedings of the 2021 International Conference on Computer Engineering and Artificial Intelligence (ICCEAI); 2021 Aug 27–29; Shanghai, China. doi:10.1109/ICCEAI52939.2021.00083.
22. Zhang L, Hua D, Zheng JH, Li Z. Two-stage robust optimization for optimal operation of hybrid hydrogen-electricity storage system considering ladder-type carbon trading. J Energy Storage. 2024;100:113473. doi:10.1016/j.est.2024.113473.